5

Study of Decoration of Reduced Graphene Oxide on Metal Oxide Based Gas Sensors

Due to certain limitation of MO_x based gas sensors, the modification in the structure of MO_x is very essential. In this regard, for enhancement of sensing response of MO_x materials, and in turn to rectify these issues related to MO_x, carbonaceous nanomaterials are greatly employed. Keeping these things in mind, this chapter focuses on p-type carbon nanomaterials for decoration on MO_x (for n-type) to improve the gas sensing response. Reduced graphene oxide (rGO) has been selected as carbonaceous nanomaterial for gas sensing, and used as decorated material on MO_x. In the first part of this chapter, rGO is decorated on ZnO nanostructures to enhance the sensing response towards hydrogen gas. Here, the main focus is to further improve the hydrogen sensing response for 4% Ni-doped ZnO nanostructures using rGO. Improved sensing response has already been discussed in the previous chapter (Ni-doped ZnO). Since, in the previous chapter, maximum relative response occurs for 4% Ni-doped ZnO, the sample discussed in this chapter has been chosen for further improvement towards hydrogen gas sensing with the help of rGO. While in the second part of this chapter, rGO has been decorated on V_2O_5 thin film to investigate the gas sensing behaviour of NO_2 gas. The structural, morphological, electrical, and gas sensing response has been systematically studied in this chapter. Lastly, the gas sensing mechanism is discussed in detail.

5.1 DECORATION OF REDUCED GRAPHENE OXIDE ON Ni-DOPED ZnO FOR THE DETECTION OF HYDROGEN GAS

Enhancement in relative response, high selectivity, and good stability of ZnO based gas sensor has become possible due to its combination with carbonaceous nanomaterials. Among all carbonaceous nanomaterials, graphene and its derivatives have gained significant attractions as gas sensors since last few decades, due to their superior qualities such as large surface to volume ratio, good chemical stability, and high electron mobility [Singh *et al.*, 2017].

However, pure form of graphene lacks surface defects sites, and has poor attachment of functional groups, which are highly responsible for excellent gas sensing properties [Jiang *et al.*, 2016]. Thus, modified graphene, which is known as reduced graphene oxide (rGO) has become the most eminent candidate in gas sensing applications [Punginsang *et al.*, 2017]. When rGO combines with MO_x or doped MO_x, it gives a new path in gas sensing applications like increase in the gas detection capability. It has been noticed that the existence of rGO in MO_x adds more defect sites on the surface for enhanced chemisorbed reaction of hydrogen to increase the sensing response. Moreover, hybrid or composite of rGO (p-type) with ZnO (n-type) will provide a p-n heterojunction that increases schottky barrier height and enhances the sensing responses [Xia *et al.*, 2017]. Anand *et al.* [Anand *et al.*, 2014] prepared Graphene/ZnO nanocomposite by in situ reduction of zinc acetate and graphene oxide (GO) to hydrogen gas. Sensor showed maximum hydrogen sensitivity of ~3.5 for 1.2 wt% graphene/ZnO composite of 200 ppm at 150˚C. Esfandiar *et al.* [Esfandiar *et al.*, 2014] fabricated Pd-WO_3 nanostructures on graphene oxide (GO) and partially reduced graphene oxide (PRGO) sheets using hydrothermal

process for the detection of hydrogen gas, and revealed ~72 sensitivity of 100 ppm hydrogen at 100˚C. Russo *et al.* [Russo *et al.*, 2012] synthesized platinum/tin oxide/reduced graphene oxide based heteronanostructures using microwave-assisted routes, and investigated the sensing response of ~3 for 1% hydrogen in air at 50 °C. Improvement in hydrogen sensing was attributed to the modulation of Schottky barrier in p-n heterojunction between SnO_2 (n-type) and rGO (p-type) including hydrogen dissociation properties of Pt by catalytic effect. Abideen *et al.* [Abideen *et al.*, 2015] fabricated the hydrogen sensor which comprised of uniformly distributed rGO loaded ZnO nanofibers, and displayed an excellent response of ~ 2524 for 10 ppm hydrogen gas at 400˚C operating temperature.

In this section, a hydrogen sensor based on Ni doped ZnO nanostructures is decorated with rGO. A simple approach such as, a drop cast method is used to decorate rGO with different concentration of Ni-doped ZnO nanostructures. The fabricated device shows enhanced relative response towards hydrogen gas at moderate operating temperature. The synergistic effect of both rGO and Ni dopant helps obtain higher relative response for hydrogen as compared to Ni doped ZnO nanostructures and rGO/ZnO based hydrogen gas sensors.

5.1.1 Experimental Setup

Ni-doped ZnO nanostructures have been deposited on p-Si (100) substrate by using RF sputtering techniques. Ni doping concentration in ZnO is optimised for hydrogen sensing as shown in the previous chapter. Sputtering parameters like RF power, Ar gas flow, substrate temperature, deposition time, and chamber pressure are maintained at 50 W, 25 sccm, 600 ^{o}C, 2 hour, and 1.5× 10^{-2} mbar, respectively. For fabrication of gas sensor, firstly Cr (10nm)/Au (200 nm) interdigitated electrodes (IDEs) has been deposited on the surface of Ni doped ZnO nanostructures using physical mask in thermal deposition method. Dimension of interdigitated electrodes is taken as 10.57×7.07 mm^2 with 11 numbers of fingers with 0.25 mm inter finger distance.

The reduced graphene oxide (rGO) which is synthesized primarily as graphene oxide (GO) using modified Hummer's method and then thermally reduced at 600°C using furnace aerosol reactor [Jiang *et al.*, 2017]. The aqueous dispersion of various rGO concentration (0 to 1.5 wt%) has been prepared by ultra-sonication of GO (9.3 mg) in toluene solvent (3.73 ml) for 8 hrs. For various concentrations (0-1.5 wt%), fabrication of different sensors is made possible when rGO flakes are decorated with 4% Ni doped ZnO nanostructures using drop cast method. In this method, 15 µl homogeneous dispersion of rGO of various concentrations with 0-1.5 wt% has been decorated on to IDEs structures. Afterwards, the sensor is annealed in the furnace at 200 ^{o}C under atmospheric conditions. Figure 5.1 depicts schematic diagram for gas sensor fabrication which includes (a) 4% Ni doped ZnO nanostructure deposited on p-Si substrate using RF sputtering and Cr/Au fabricated IDEs, (b-c) Drop cast method used to decorate rGO over Ni doped ZnO nanostructures for sensor fabrication. Thus, various rGO concentrations (0-1.5 wt%) loaded with Ni doped ZnO nanostructure based gas sensors have been fabricated for hydrogen gas sensing.

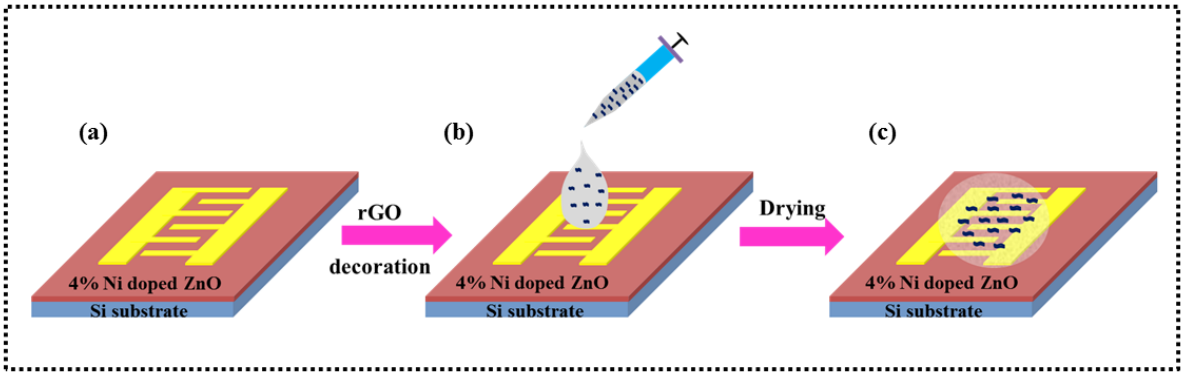

Figure 5.1: Schematic diagram for gas sensor fabrication which includes (a) Ni doped ZnO nanostructure deposited on p-Si substrate using RF sputtering with IDEs (b-c) Drop cast method used to decorate rGO over Ni doped ZnO nanostructures

5.1.2 Structural Properties of rGO Decorated Ni-doped ZnO Nanostructures

Figure 5.2 (a-b) shows XRD spectra of Pristine and 0.75 wt% rGO loaded Ni doped ZnO nanostructures. Figure 5.2 (a) gives a clear picture about crystalline growth of 4% Ni doped ZnO comprising of c-axis due to the presence of strong peak of (002) plane at 2θ position ~34.6° along with two others peak corresponding to (101) and (102) planes. With 0.75 wt% rGO loading on 4% Ni doped ZnO, XRD spectra shows one slight peak at 2θ position 24.43°, which demonstrates the presence of (002) plane of rGO.

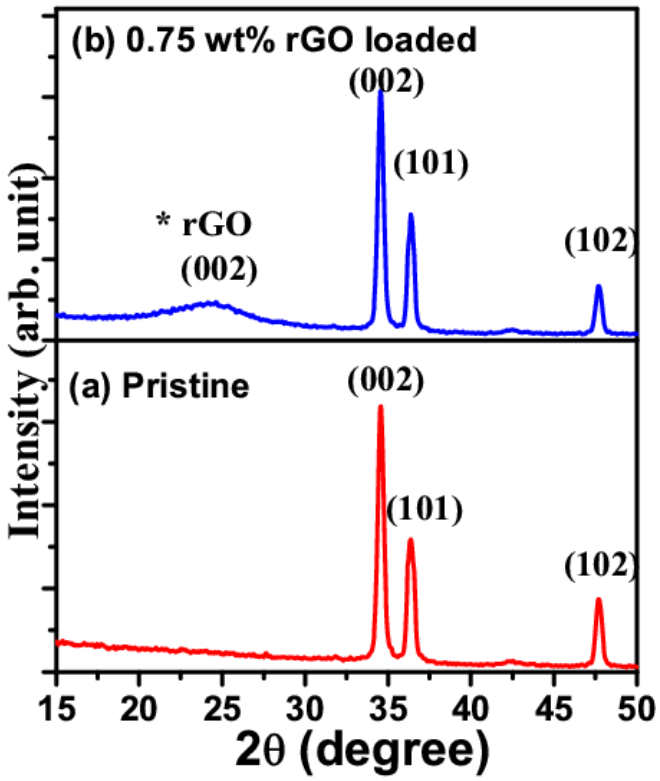

Figure 5.2: (a-b) XRD spectra of Pristine and 0.75 wt% rGO loaded Ni doped ZnO nanostructures

It is observed that rGO loading on the Ni doped ZnO nanostructures did not degrade the crystallinity of ZnO. Raman spectra of pristine and 0.75 wt% rGO loaded Ni doped-ZnO nanostructures are shown in Figure 5.3 (a-b).

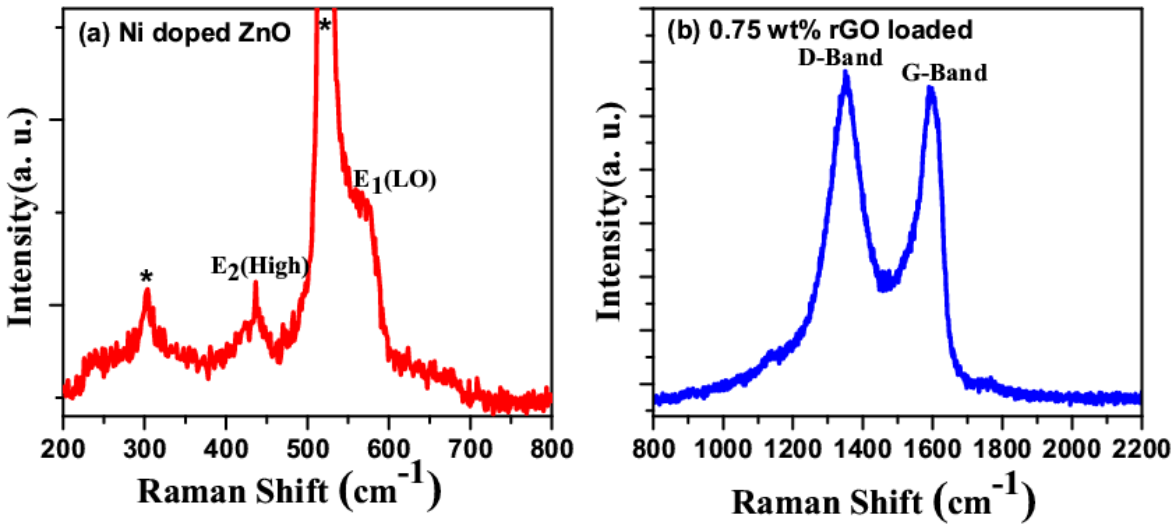

Figure 5.3: (a-b) Raman spectra of pristine and 0.75 wt% rGO samples

Raman spectra shows the crystalline growth of nanostructures due to the presence of two peaks which represents the presence of two optical phonon modes: E_2 (High) at ~475 cm^{-1} and E_1(LO) at ~582 cm^{-1}. The remaining peaks in this spectra show the Si substrate. Raman spectra of 0.75 wt% rGO loaded Ni doped ZnO nanostructures have been illustrated in Figure 5.3 (b). Raman spectra of 0.75 wt% provides two strong peaks corresponding to D-band (1349 cm^{-1}) and G-band (1596 cm^{-1}) [Kathiravan *et al.,* 2017; Liu *et al.,* 2017]. The ratio of these D-band and G-band intensities (I_D/I_G~1.03) indicates about the disorder degree and average size of sp^2 domains present in rGO.

5.1.3 Morphological Analysis of rGO Decorated Ni-doped ZnO Nanostructures

Furthermore, surface morphology has been studied using SEM techniques. Digital photograph of the gas sensor is shown in Figure 5.4 (a) where Cr/Au IDEs structure shows gas sensing applications.

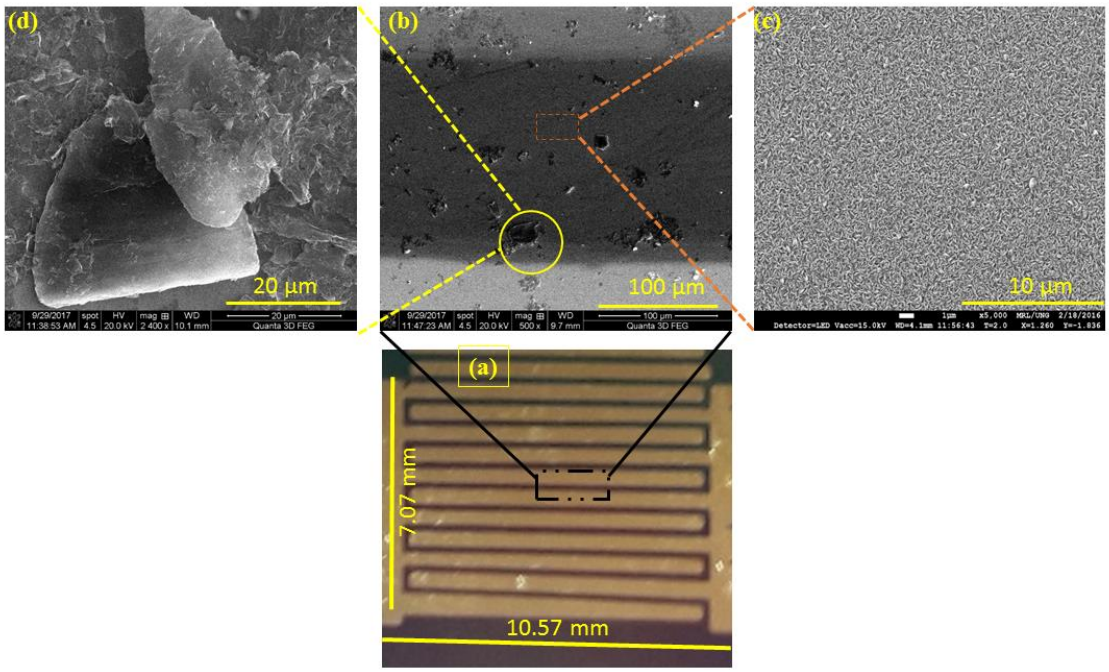

Figure 5.4: (a) Digital photograph of the gas sensor with Cr /Au IDEs structure for gas sensing applications and the magnified SEM images (b-d) Two Cr /Au electrodes lines of IDEs structures, Ni doped ZnO nanostructures, and 0.75 wt% rGO loaded ZnO, respectively

The magnified SEM images of two Cr/Au electrode lines of IDEs structures can be seen in Figure 5.4 (b). An uneven distribution of rGO flakes between two electrodes is caused by drop casting of 0.75 wt% rGO. The magnified image of decoration of 0.75 wt% rGO over Ni doped ZnO nanostructures is shown in Figure 5.4 (c-d). It is clearly seen that Ni-doped ZnO nanoplates are deposited by RF-sputtering technique which is uniformly distributed throughout the substrate. However, synthesis of rGO by Hummer method and drop casting will result in uneven distribution of rGO with larger size over the ZnO surface.

5.1.4 Electrical Characterization of rGO Decorated Ni-doped ZnO Nanostructures

In the previous chapter, it is mentioned that the performance of sensor and its selectivity towards hydrogen can be enhanced with minimum limit of detection ~1ppm due to doping of Ni into ZnO nanostructure up to an acceptable limit (4% Ni in that case). In order to further enhance sensor's response, 4 % Ni doped nanostructures has been functionalized with various concentrations of rGO flakes loading. This could be a promising strategy to increase the sensor's performance.

Enhanced relative response could be attributed to the formation of various heterojunctions between rGO and Ni doped ZnO. Effect of loading various rGO concentrations (0.25 wt% to 1.5 wt%) on sensor's electrical properties has been studied by measuring *I-V* characteristics. Figure 5.5 (a-b) shows room temperature current voltage (*I-V*) characteristics of various concentration (0.25 wt% to 0.75 wt%) of rGO loaded sensor, and highest concentration of rGO (1.5 wt%) sample, that have been measured, respectively.

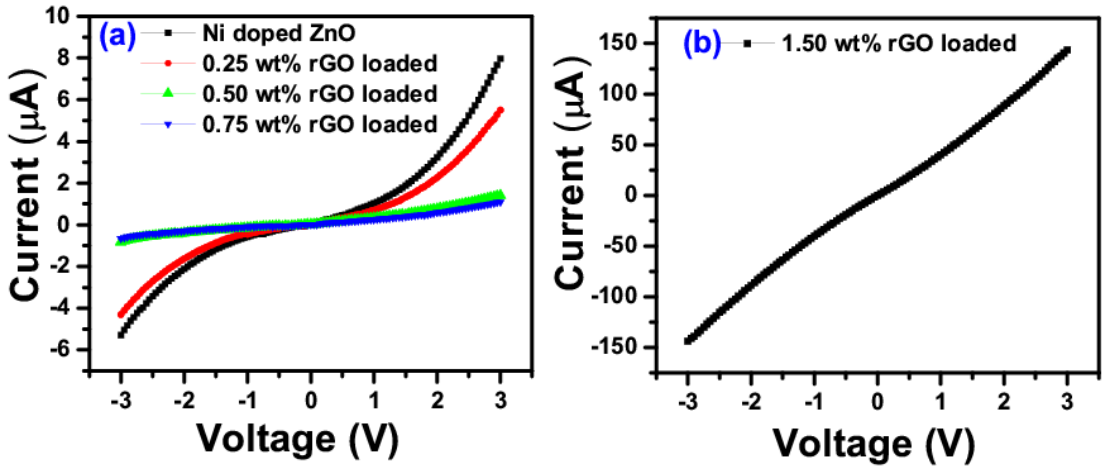

Figure 5.5: Room temperature *I-V* characteristics of various concentration (0.25 wt% to 0.75 wt%) of rGO loaded sensor and highest concentration of rGO (1.5 wt%) sample, respectively

Pristine sample shows rectifying behaviour due to the presence of large Schottky barrier height at Metal- ZnO junctions which have already been observed in the previous chapter. However, with increasing rGO concentrations from 0.25 wt% to 1.5 wt% there is high influence of current conduction. Initially, up to low concentration limit of 0.75 wt% rGO, sensor shows decrease in current from 7.97 μA to 1.11 μA at 3V forward bias voltage. This reduction in current conduction indicates the increase in sensor's resistance as rGO loading concentration increases from 0.25 wt% to 0.75 wt%.

Change in sensor resistance can be understood by charge transfer theory where work function of rGO (4.4 eV- 5.0 eV) is much higher than ZnO (~4.3 eV) [Lee *et al.*, 2015; Yin *et al.*, 2010]. As a result, a number of Schottky hetero-junctions have been formed at interface of n-ZnO and p-type rGO. During current conduction, the electrons will move from ZnO to rGO causing increase in sensor's resistance due to formation of Schottky junction which has resemblance with *I-V* characteristic shown in Figure 5.5 (a). Further increase in rGO concentration up to 1.5 wt%, sudden increase in sensor's current has been observed. The main

reason behind current conductions is due to the formation of conduction path between two IDE electrodes while loading of large rGO concentration on Ni doped ZnO nanostructures [Venkatesan *et al.*, 2016]. Therefore, the sensor shows enhanced current conduction as shown in Figure 5.5 (b).

5.1.5 Gas Sensing Studies of rGO Decorated Ni-doped ZnO Nanostructures

In order to measure the sensor's response towards hydrogen, various concentrations of rGO (0 to 1.5 wt%) loaded Ni doped ZnO nanostructures sensors have been fabricated, and a series of gas sensing tests has been performed to investigate the sensor's response towards target gas. For gas sensing applications, sensor's relative response, operating temperature, and gas concentration are the primary factors. Gas sensing principle of MO_x is based on surface phenomenon where adsorption/desorption of the target gas on the surface of sensing material plays an important role in the sensor's performance. Sensor's relative response is recorded by measuring the relative change in resistance of the sensor in presence of target gas with respect to the resistance in air. In order to demonstrate the effect of rGO concentrations on sensor's performance for hydrogen gas, sensor's relative response curve for pristine and various (0.25 wt%-1.5 wt%) concentrations of rGO loaded Ni-ZnO nanostructures for 100 ppm hydrogen concentration at moderate operating temperature of 150 °C has been performed, and the results are shown in Figure 5.6.

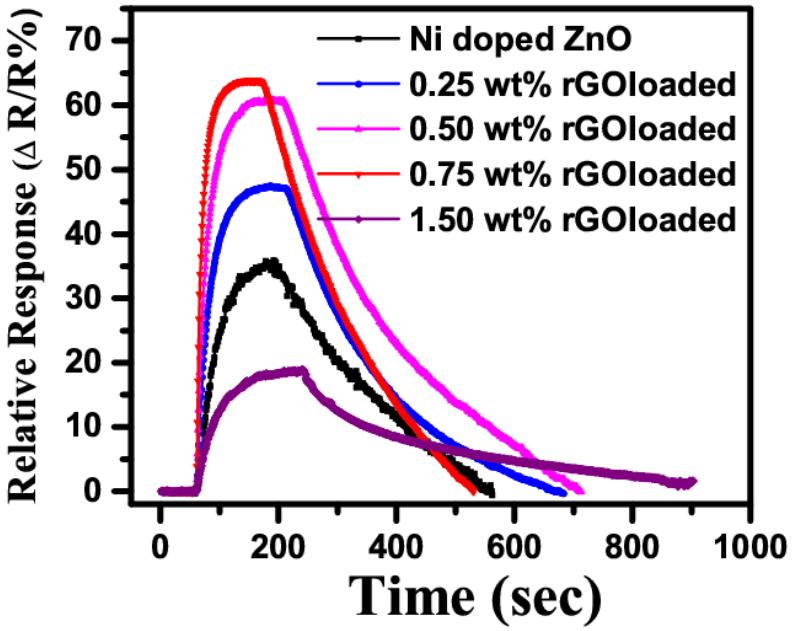

Figure 5.6: Sensor's relative response for pristine and rGO loaded ZnO for 100 ppm hydrogen gas at 150 °C operating temperature

It can be clearly seen that with increasing concentration of rGO flakes from 0 to 0.75 wt%, the relative response increases from 35.37% to 63.8% at 150 °C for 100 ppm hydrogen gas concentration. Further increasing the rGO concentration to 1.5 wt%, there is drastic decrease in sensor's relative response ~19.1% even at same operating conditions and concentrations. Thus, optimized rGO loading concentration (0.75 wt%) can double fold the enhanced sensor's response as compared to pristine ZnO. As discussed earlier in electrical characterization, intrinsically rGO and ZnO shows p-type and n-type behaviour, respectively.

According to the charge transfer theory, Fermi-level alignment takes place and band bending is present during rGO-ZnO heterojunction formation. Such type of Schottky junctions plays an important role in gas sensing. Therefore, rGO loading up to optimum concentration can increase sensor's relative response which is due to the formation of various p-n heterojunctions at the interface of rGO and ZnO material, which further improves the active sites for oxygen atom adsorption. The rGO extracts electrons from ZnO, which increases the width of the depletion region, and also provides active sites (due to defects) to enhance oxygen

molecule adsorption on the surface. Sensor's resistance increases with loading of hydrogen because it reacts with adsorbed oxygen molecules present at both rGO and ZnO surface, that reduces the junction barrier to a large extent. However, further increase in rGO concentration up to 1.5 wt% might cover maximum surface active sites of ZnO, that consequently reduce the surface adsorbed oxygen molecules. Thus, overall gas sensor performance is drastically reduced as compared to pristine sample. Different concentration of hydrogen gas from 1ppm to 100 ppm has been exposed on the sensor's surface, and studied systematically. Figure 5.7 shows sensor's relative response for 1 ppm to 100 ppm hydrogen at 150 °C operating temperature (a) 0.75 wt% rGO loaded and (b) comparative studies for all rGO loaded sensor's response.

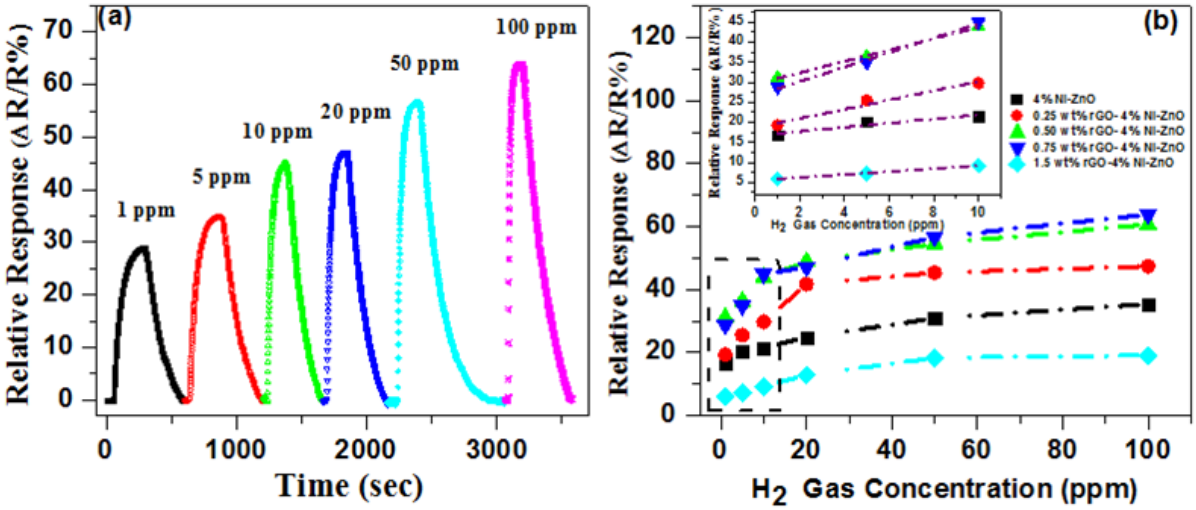

Figure 5.7: Sensor's relative response from 1ppm to 100 ppm at 150 °C operating temperature for (a) 0.75 wt% rGO loaded sensor and (b) comparative studies for all rGO loaded sensors and where, the inset figure represents the enlarged linear fitted hydrogen gas sensing response from 1 to 10 ppm

It is noticed that 0.75 wt% rGO loaded sensor demonstrated efficient sensor response (~28.74%) even in the presence of lowest hydrogen concentration of 1ppm. With increasing hydrogen gas concentration up to 100 ppm, sensor's relative response also increases up to ~ 63.8%, attributed to enhance desorption reactions which provide larger change in junction depletion layer and surface conductivities. Figure 5.7 (b) shows relative study of various rGO loaded sensor's response with increasing hydrogen concentration. With optimum rGO loading concentration (0.75 wt%) with respect to pristine sensor, sensor's response efficiently enhances from 16.76% to 28.74% at 1ppm. Sensor's relative response depicts almost linearly increasing response pattern for all sensors when gas concentration is 1 ppm, 5 ppm, 10 ppm and 20 ppm, respectively, **w**here the inset figures in Figure 5.7 (b) represent the enlarged linear fitted hydrogen gas sensing response from 1 to 10 ppm. With higher gas concentration, drastic improvement in gas sensor response has been recorded for all sensors. Moreover, oversaturated rGO concentration (1.5 wt%) can reduce sensor's response up to 19.1% with respect to 0.75% rGO loaded sensor response (~63.8%) for 100 ppm hydrogen. Selectivity of gas sensor towards target gas molecules is also a key parameter which is required to check the sensor's performance. The selectivity of various rGO loaded sensors have been studied and shown in Figure 5.8.

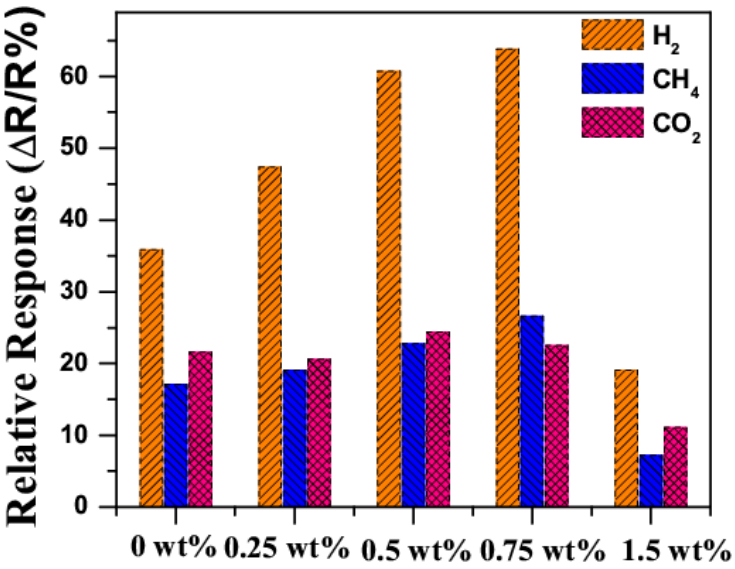

Figure 5.8: Selectivity histogram for Pristine and rGO loaded Ni doped ZnO nanostructures based sensor

It shows the sensor response towards various target gases including hydrogen, CH_4 and CO_2 at 100 ppm. Although pristine sensor also shows high sensor response towards hydrogen in comparison to CH_4 and CO_2 gases at 100 ppm. With optimized 0.75 wt% rGO concentration sensor become highly selective towards hydrogen with approximately three-fold increase in sensor's relative response (~63.8%) with respect to CH_4 (~26.5%) and CO_2 (~22.5%) target gases. The comparison of gas sensing performance for doped ZnO and rGO loaded ZnO sensors with present work for various target gas concentrations has been shown in Table 5.1.

Table 5.1: Comparison of gas sensing performance of previously reported doped ZnO, and rGO loaded ZnO sensors, and present work for various target gases concentrations

Sl No.	*Sample*	*Working temperature (°C)*	*Target gas(ppm)*	*Response time (s)*	*Response (S)*	*References*
1	Mg doped ZnO film	300	H_2 (5000)	-	50[a]	Liu *et al.*, 2011
2	Ti doped ZnO tetrapods	260	ethanol (100)	90	11[a]	Zheng *et al.*, 2010
3	ZnO p-n homojunction	400	H_2 (1000)	146	1.15[a]	Hazra *et al.*, 2006
4	Na doped ZnO nanorods K doped ZnO nanorods	280 300	ethanol (100) ethanol (100)	56 45	37.8[a] 45.2[a]	Saaedi *et al.*, 2017
5	Cd doped ZnO nanrods	80	H_2 (500)	43	1.67[d]	Yang *et al.*, 2015

6	Graphene/ZnO nanocomposites	150	H_2 (200)	22	3.5[a]	Anand *et al.*, 2014
7	ZnO/In2O3 core-shell nanorods	RT	H_2 (500)	-	20.5%[c]	Huang *et al.*, 2012
8	In doped ZnO thin film	300	H_2 (5)	-	15%[b]	Pati *et al.*, 2015
9	rGO decorated Ni doped ZnO nanostructures	150	H_2 (100)	28	63.8%[b]	This work

[a] $S = R_{air}/R_{gas}$, [b] $S = (R_{air}-R_{gas})/R_{air}$ x100%, [c] $S = |(R_{H2}-R_{air})/R_{air}|$x100%, [d] $S = R_{N2}/R_{gas}$

When comparing with other reported sensors on either doped ZnO nanostructures or rGO loaded ZnO nanostructures, the sensor based on rGO decorated 4% Ni-doped ZnO exhibit moderate sensor response (~ 63.8 %) and fast response time (28 sec) even for 100ppm hydrogen gas concentration at moderate operating temperature (150 °C).

5.1.6 Gas Sensing Mechanism

Gas sensing mechanism for MO_x is basically surface phenomenon which strongly depends on adsorption/desorption of target gases which leads to change in the sensor resistance. In presence of air, oxygen molecules are adsorbed on Ni doped ZnO nanostructure surface and creates adsorbed oxygen ions species (O^-, O_2^-) by extracting conduction band electrons, creating a space charge conduction region. On loading the target gases, they react with these adsorbed oxygen species, and conduction band electrons return that in turn, reduces the space charge width. This loading of hydrogen causes large change in depletion region of metal oxides (ZnO). In this study, rGO also plays a significant role in hydrogen gas sensing. The combined effect of rGO loaded 4% Ni-ZnO sensor has been demonstrated in gas sensing mechanism. Figure 5.9 (a-b) shows the schematic diagram of gas sensing mechanism in presence of air as well as hydrogen for rGO loaded 4% Ni-ZnO nanostructures and the illustration of band diagram rGO/ZnO heterojunction before contact and after contact (in air, in hydrogen) is represented in Figure 5.9 (c-e).

Mechanistically, gas sensing is highly influenced by Ni doped ZnO nanostructures and formation of various rGO/ZnO Schottky barriers. On the other hand, it can be understood by p-n heterojunction due to the presence of p-type and n-type nature of rGO and ZnO, respectively. The maximum number of heterojunctions is formed at the interface between ZnO and rGO at the optimum condition when rGO concentration is around 0.75%. The concept behind formation of Schottky barrier at rGO/ZnO heterojunction can be explained by charge transfer theory [Lee *et al.,* 2015; Liu *et al.,* 2017]. Due to the presence of large difference in Fermi-level positions of rGO and ZnO, the work function of rGO has a higher value than ZnO work function, as shown in Figure 5.9 (c). rGO always has zero bandgap which makes it behave like a metallic junction similar to the metal semiconductor schottky junction [Van Quang *et al.,* 2014]. In p- type rGO, the majority charge carriers are holes. In contrast, the electrons are majority charge carriers in n-type ZnO. When rGO and ZnO materials combine together, the holes move from rGO to ZnO, and electron conduction takes place from n-ZnO to p-rGO at the interface between ZnO and rGO. Consequently, the charge migrations from the both material will neutralize the opposite charge at the interface, which leads to the formation of thick depletion layer between ZnO and rGO. After that, the total carrier concentration decreases. This results in increased resistance in air, which is confirmed by *I-V* characteristics of 0.75 wt% rGO as shown in Fig 5.5 (a).

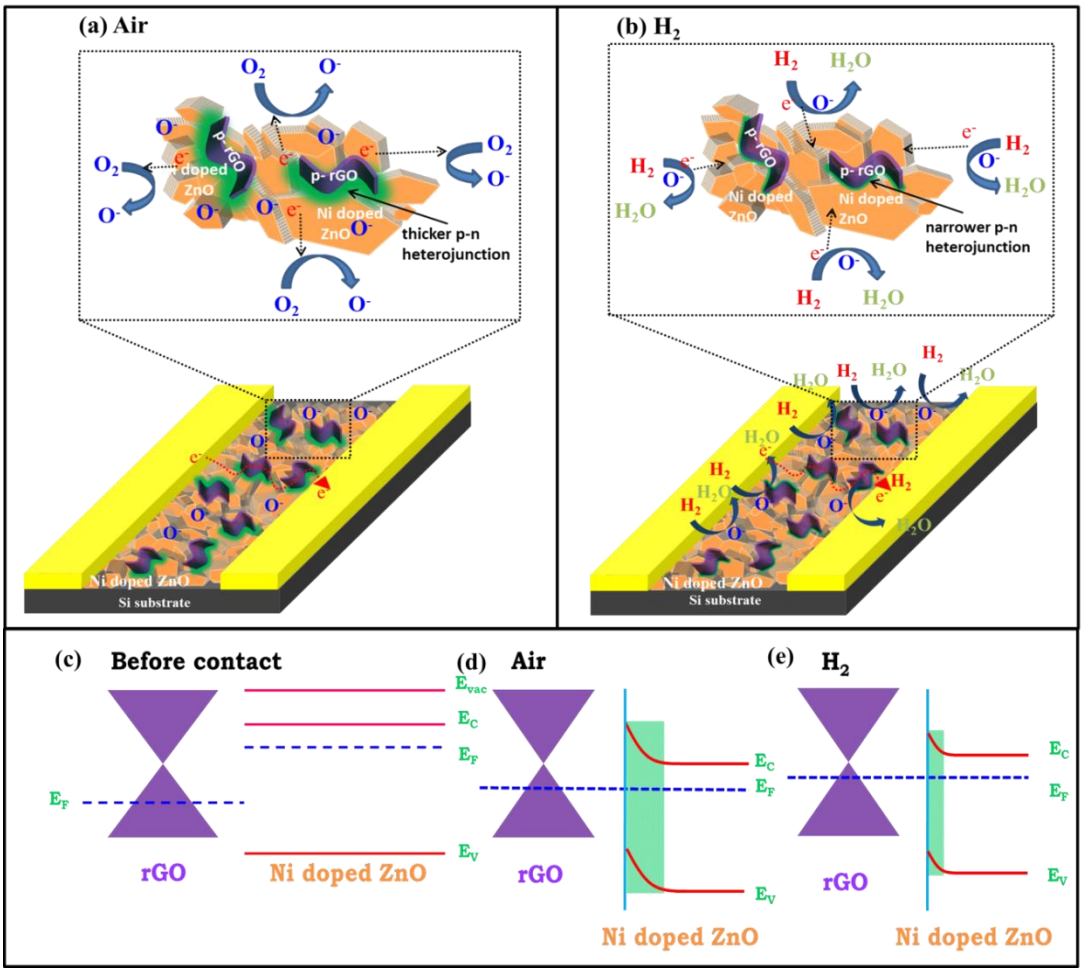

Figure 5.9: (a-b) Schematic diagram of gas sensing mechanism in presence of air and hydrogen for rGO loaded 4% Ni-ZnO nanostructures and (c-e) The band diagram illustration of rGO/ZnO heterojunction before contact and after contact (in air, in hydrogen)

In view of band diagrams of ZnO and rGO, when both charge carriers are migrated till fermi-level comes into level and band bending takes place due to formation of Schottky barrier at heterojunctions as shown in Figure 5.9 (d-e). Therefore, after exposure to these heterojunctions in the air (oxygen atmosphere), electrons get extracted from the conduction band and increase the space charge region width at heterojunction as oxygen molecules get adsorbed on both ZnO as well as defects site of rGO. When these heterojunctions get exposed to hydrogen gas, hydrogen molecules react with adsorbed oxygen ions and release conduction band electrons back to the conduction band, which reduces Schottky barrier height while free electrons also flow back from rGO to ZnO. Thus, the combined effect of various p-n Schottky junction formation and availability of Ni doped ZnO nanostructures surface reaction area makes these (0.75%) rGO loaded sensor highly efficient towards hydrogen sensing with lowest detection limit of 1ppm. Apart from this, rGO has defect sites and functionalized groups on its surface which acts as active sites for the gas, and hence the relative response is increased. Moreover, when the concentration of rGO is increased up to ~ 1.5 wt%, these rGO agglomerates and formation of interconnection between the electrodes decreases the sensor's resistance. In addition, other factors such as p-n heterojunction and chemisorbed oxygen ions due to active sites of Ni-ZnO are less effective because of the availability of least surface reaction sites. Therefore, higher concentration of rGO would decrease the hydrogen sensing relative response. To sum up, the enhanced sensor's relative response and better selectivity can be achieved by incorporating surface modification via loading of rGO over Ni doped ZnO sensor.

5.2 rGO DECORATED V_2O_5 THIN FILM FOR NO_2 DETECTION

In the second section of this chapter, enhancement in sensing response film towards Nitrogen dioxide (NO_2) based on rGO decorated V_2O_5 thin has been discussed. NO_2 is one of the most common air pollutants in the environment which is emitted from industrial waste, automobile by-products, and power plants [Garciduenas *et al.,* 2002; Liu *et al.,* 2014; Afzal *et al.,* 2012]. Further, the formation of acid rain occurs when NO_2 interacts with water molecules in the atmosphere; that bring about serious harm to the ecosystem [Zhang *et al.,* 2004]. Moreover, the continued inhalation of NO_2 causes throat irritation, lung infections and decreases the capability of the respiratory system [Tamaekonga *et al.,* 2014]. Therefore, the development of highly sensitive and selective NO_2 gas sensors is greatly required for timely detection of the harmful gases even at extremely low concentration ~1 ppm. In order to suffice the demand of excellent gas sensors, the need of MO_x based gas sensors for precise detection of NO_2 gas emerges [Lee *et al.,* 2018]. Vanadium pentoxide (V_2O_5) is n-type MO_x, also demonstrates excellent sensing properties in terms of sensitivity, selectivity, and cost-effectiveness. Apart from this, the functional groups attached on the rGO surface are also useful to boost the sensing response. Both the pure form of V_2O_5 and graphene are not enough to give excellent sensing response and selectivity. Therefore, the combination of V_2O_5 and rGO may have good capability to enhance the sensing response at low operating temperature. Lee *et al.* [Lee *et al.,* 2015] showed improved NO_2 sensing properties based on n-type nanofibers loaded on p-type rGO nanosheets. The sensor showed 20 times higher sensing response than pure SnO_2 nanofibers. The excellent sensing response was suggested by the formation of local p-n heterojunctions between p-type rGO nanosheets and n-type nanofibers. Zhang *et al.* [Zhang *et al.,* 2017] demonstrated NiO-rGO and ternary NiO-SnO_2-rGO nanocomposites for NO_2 gas sensing. Both samples were compared, and it was reported that ternary nanocomposites show superior response of 60 ppm NO_2 at RT under equal specific surface area which indicates vital performance of the heterojunction. Jie *et al.* [Jie *et al.,* 2015] fabricated graphene wrapped WO_3 nanosphere composite using sol-gel method. The sensor exhibited sensing response of ~40.8% on exposure to 56 ppm NO_2. However, for pure form based sensor like, pure WO_3 and graphene sensors; no response was observed. Tammanoon *et al.* [Tammanoon *et al.,* 2015] prepared flame-spray-made undoped SnO_2 nanoparticles and loaded it with 0.1-5 wt% electrolytically exfoliated graphene. Then sensors were employed to detect NO_2 gas at low working temperatures; they could obtain the maximum sensing response with 0.5 wt% graphene at 150 °C.

In this part of the chapter, a NO_2 sensor based on rGO decoration on V_2O_5 thin film has been discussed. Facile route (drop cast) is used for the decoration of rGO on DC sputtered grown V_2O_5 thin film. The proposed sensor shows elevated NO_2 sensing response at mild working temperature. It could be perceived that the combined effect of V_2O_5 and rGO come up with superior NO_2 sensing response than the effect offered by V_2O_5 sensor.

5.2.1 Experimental Setup

Around 100 nm thick V_2O_5 thin film has been deposited on Si_3N_4 (300 nm thick)/n-Si (100) using DC sputtering (Anelva SPF -332H). The growth of Si_3N_4 on n-Si (100) substrate is carried out using PECVD (OXFORD INSTRUMENTS). Prior to the deposition of Si_3N_4, the n- Si substrate is degreased in organic solvents such as trichloroethylene, acetone and methanol at 70 °C for 5 min, respectively, followed by chemical cleaning in 5% HF to remove the surface oxide and then n- Si was rinsed with de-ionized water, and subsequently dried with nitrogen gas. Finally, 300 nm thick Si_3N_4 thin films have been deposited at 250 °C. The deposition of V_2O_5 thin film is carried out from a 99.99% pure vanadium metal target. The sputtering chamber was pumped down to 1.2×10^{-6} mbar prior to heating of the substrate, and then the substrate temperature was raised to 450 °C at which the deposition of V_2O_5 was performed. During deposition, the pressure of the chamber was kept at 3×10^{-3}mbar. The argon flow rate, O_2 flow rate, and DC power were kept at 5 sccm, 0.05 sccm, and 100 W, respectively. The distance between the target and the substrate was kept at 10 cm. On the other hand, the synthesis of GO is accomplished by natural graphite flakes via Hummer's method [Raliya *et al.,* 2017]. Initially, graphene oxide nanosheet is synthesized by a precursor powder of graphitic oxide. Then the

powder is poured into sulphuric acid and potassium permanganate. Furthermore, the water and hydrogen peroxide has been mixed to make suspension, which later reduces to residual permagnate. This suspension is separated out by using 0.45 micron size whatman filter paper. Ultrasonication then, helped to exfoliate the graphene oxide sheets. Finally, the sheets are filtered out numerous times, and subsequently made to go through the centrifugation process. Then, GO has been annealed at 600˚C by furnace aerosol reactor, and transformed into rGO [Jiang *et al.*, 2017]. Further, after fabricating interdigitated electrode (IDE) patterns, the gas sensing measurement of rGO decorated V_2O_5 thin film has been implemented. IDE pattern with 10 µm wide fingers and 10 µm wide pitch is fabricated by depositing Au metal (thickness ~200 nm) using RF sputtering followed by standard photolithography (Suss MicroTec Mask Aligner), and wet chemical etching processes. Furthermore, 30µL of rGO solution (2mg L^{-1}) has been decorated on IDE pattern and dried at 90˚C. The schematic diagram of various fabrication steps for final device is demonstrated in Figure 5.10.

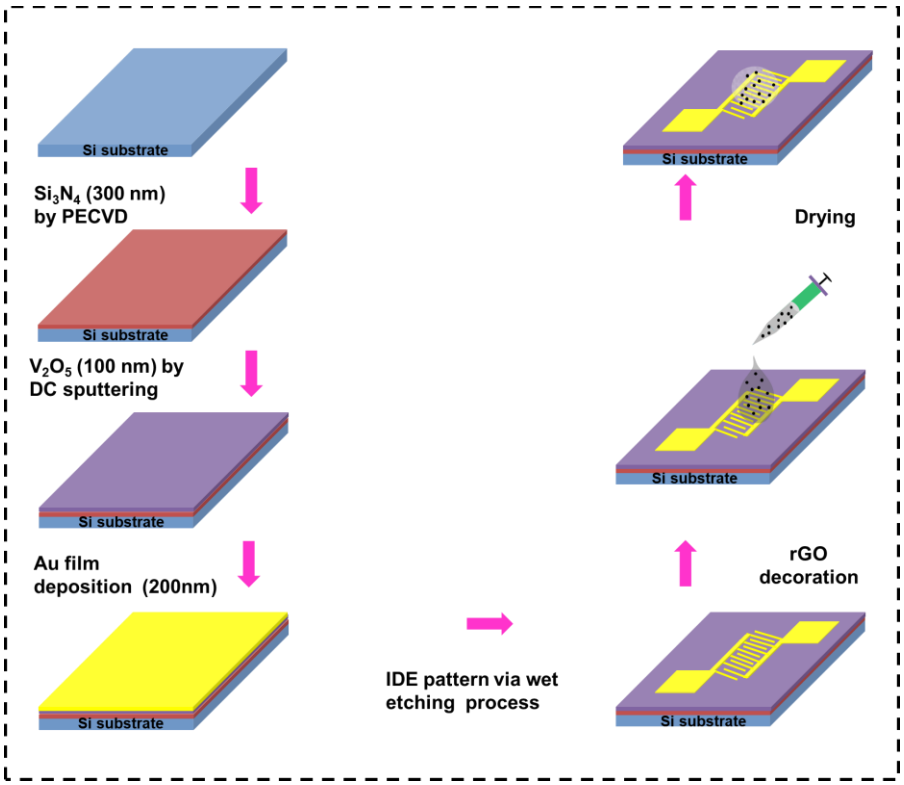

Figure 5.10: Schematic diagram of various fabrication steps for final device

Optical image of the IDE pattern thus obtained is shown in the Figure 5.11. Apart from this, the rGO film has been deposited on IDE pattern fabricated glass substrate.

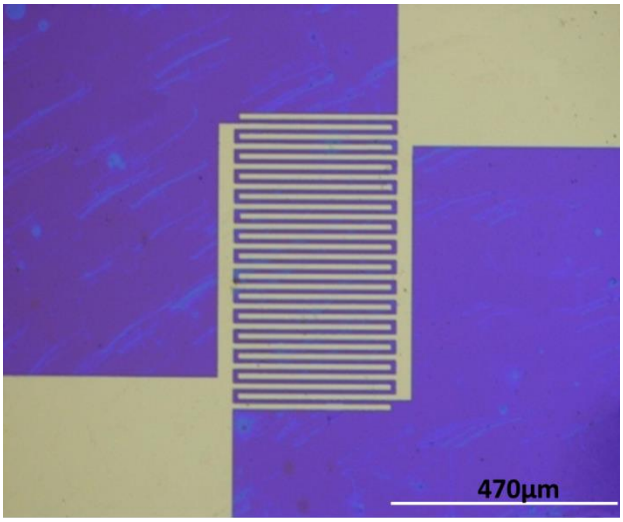

Figure 5.11: Optical image of IDE pattern on V_2O_5 thin film

5.2.2 Structural Characterization

Structural characterization of the V_2O_5 thin film has been evaluated using XRD. Figure 5.12 shows a 2θ scan of grown V_2O_5 thin film on Si_3N_4/Si(100). The peaks at 2θ= 14.62˚, 19.03˚, 30.35˚, and 40.09˚, are related to the (020), (001), (040), and (002) planes of the V_2O_5, which confirm the growth of V_2O_5 thin film.

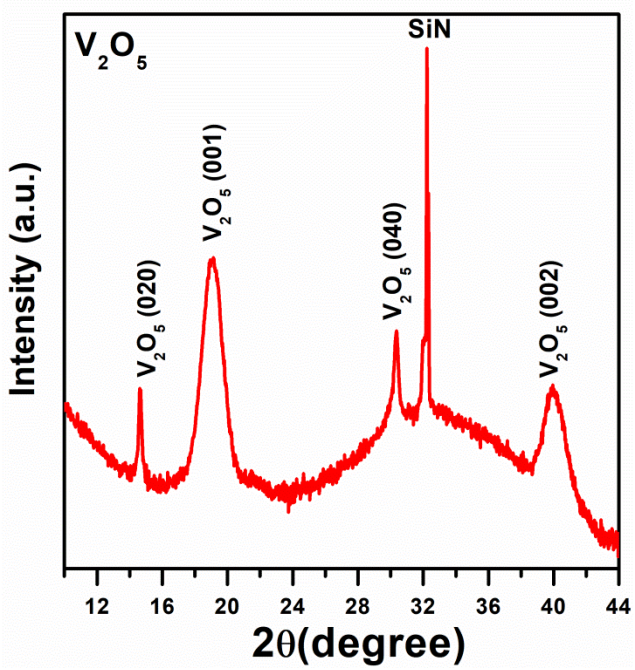

Figure 5.12: XRD pattern of the V_2O_5 thin film

5.2.3 Chemical Composition of rGO Decorated V_2O_5 Thin Film

In order to acquire the information about chemical composition of rGO decorated V_2O_5 thin film, the XPS characterization has been carried out which determines the chemical composition of vanadium and oxygen and carbon. Figure 5.13 (a) shows the core level spectra of V $2p_{3/2}$ and V $2p_{1/2}$ binding energies as assigned to 516.8 and 524.1eV of V_2O_5, respectively, displaying that vanadium is mainly present in the +5 oxidation state [Modafferi *et al.*, 2012].

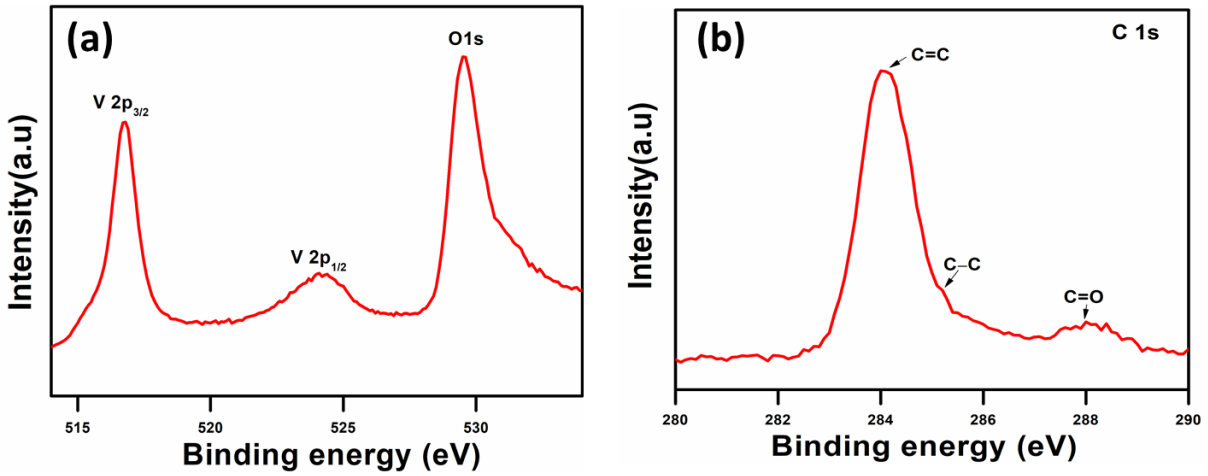

Figure 5.13: XPS spectra of rGO-decorated V_2O_5 thin films: (a) V 2p and O 1s and (b) C 1s

Moreover, the characteristics peak at O1s which is centered at 529.5eV indicates that the oxygen is bonded with the V in V_2O_5 thin film. The XPS spectra of rGO indicates the C1s peaks which contain C=C (284 eV), C-C (285.2 eV), and C=O (288 eV) as displayed in Figure 5.13 (b) [Yu *et al.*, 2014].

5.2.4 Topography Analysis

Figure 5.14 shows 3×3 µm² scanned Atomic Force Microscopy (AFM) image of V_2O_5 thin film, which illustrates a smooth film, and gives 6.5 nm RMS roughness of the film.

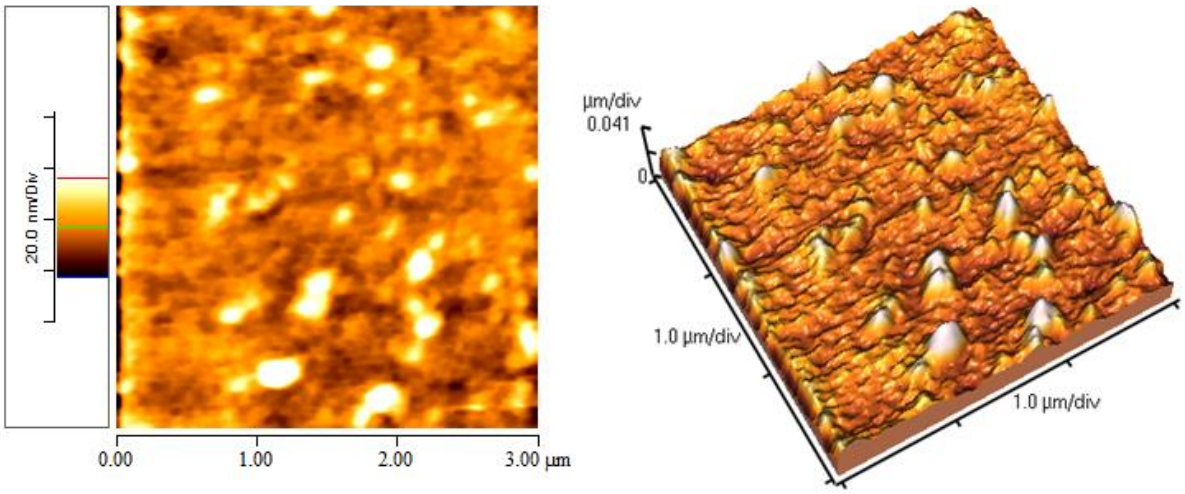

Figure 5.14: AFM images of V_2O_5 thin film

5.2.5 Work Function Analysis

The work function of rGO and V_2O_5 thin film has been measured using scanning Kelvin probe system under ambient environment, as shown in Figure 5.15 (a-b).

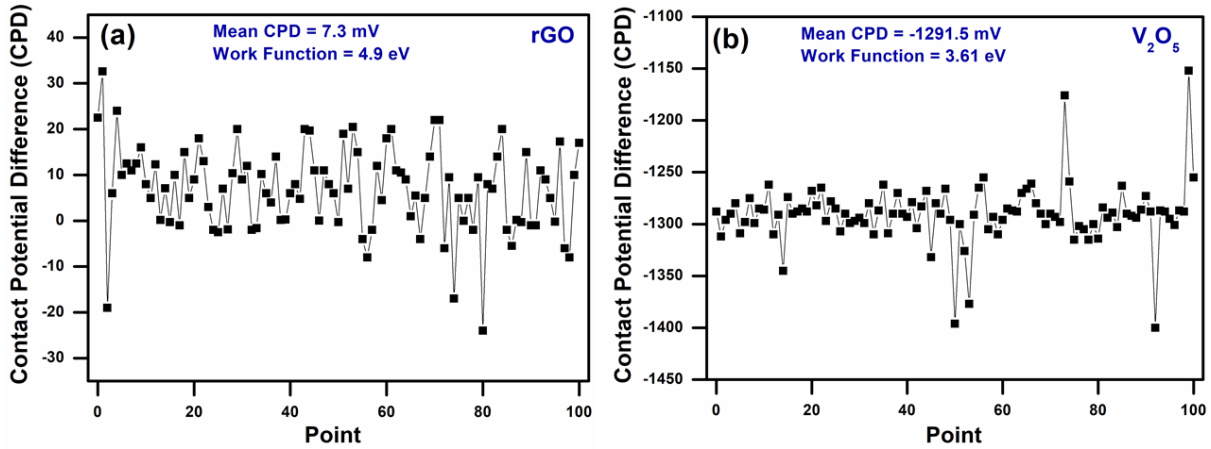

Figure 5.15: Contact potential difference (V_{CPD}) of (a) rGO and (b) V_2O_5 thin film as a function of number of points taken during the work function estimation

Au tip is used to scan the sample in non-contact mode where the workfunction of Au tip is ~ 4.9eV and tip size is ~1.83 mm diameter. Moreover, 2 mm distance on the sample is selected during the Kelvin probe measurement. Figure 5.15 (a-b) shows the contact potential difference (V_{CPD}) of (a) rGO and (b) V_2O_5 thin film with respect to number of points taken during the work function calculation. 100 points has been observed at the same distance by vertically vibrating the tip to calculate the contact potential difference to rGO and V_2O_5, respectively. After that, the contact potential difference (V_{CPD}) of rGO is measured to 7.3 mV whereas; V_{CPD} of V_2O_5 is around -1291.5mV. Therefore, the work function of rGO and V_2O_5 is calculated as 4.90 and 3.61eV using the Eq. (5.1).

$$\phi_{sample} = \phi_{Au} + e(V_{CPD}) \tag{5.1}$$

5.2.6 Electrical Characterization

Furthermore, the effect of rGO on V_2O_5 thin film has been compared with *I-V* characterization at room temperature. Moreover, *I-V* curve for V_2O_5 thin film, rGO decorated V_2O_5 thin film, and rGO film has been investigated at room temperature as shown in Figure 5.16.

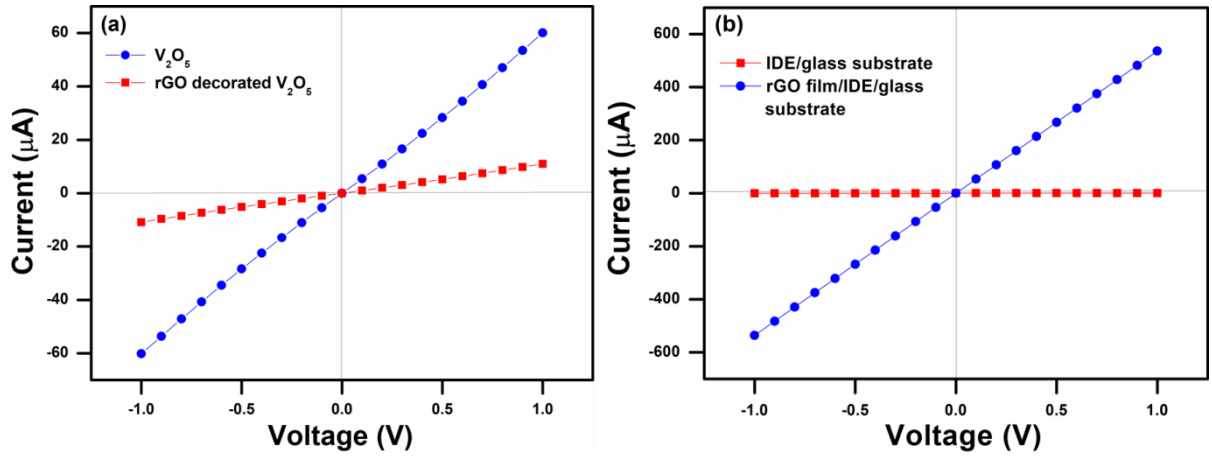

Figure 5.16: Room-temperature *I–V* characteristics of (a) V_2O_5 thin film and rGO-decorated V_2O_5 thin film and (b) rGO thin film/IDE/glass substrate

It can be seen that the current conduction behavior is largely affected by the decoration of rGO concentration than V_2O_5 thin film. At first, rGO decorated V_2O_5 sensor shows a decrease in current from 60μA to 10μA at 1 V as shown in Figure 5.16 (a). The drop in current is mainly due to the increased resistance after rGO decoration on V_2O_5 thin film, and can be understood by electron transfer mechanism in p-n heterojunctions. The formation of p-n heterojunction will

happen when p-type rGO and n-type V_2O_5 combine together, where the workfunction of rGO, and V_2O_5 are 4.90, and 3.61 eV, respectively. Consequently, the electron movement would take place from n-type V_2O_5 to p-type rGO until their Fermi level is aligned. This formation decreases the carrier concentration in rGO as well as V_2O_5 thin film. Furthermore, decreased current is observed in air. However, current has been enhanced drastically for rGO thin film shown in Figure 5.16 (b). The increase in current is attributed to the highly conducting rGO film placed between the IDE electrodes on glass substrate. It correspondingly offers less resistance as compared to rGO decorated V_2O_5 thin film.

5.2.7 Gas Sensing Measurement

Sensing response of the V_2O_5 thin film and rGO decorated V_2O_5 thin film has been tested for different concentrations of NO_2. Generally, the gas concentration and working temperature highly affecting the MO_x based gas sensors. Figure 5.17 (a-e) shows the relative response of V_2O_5 thin film towards NO_2 gas from 1 to 100 ppm at different temperatures.

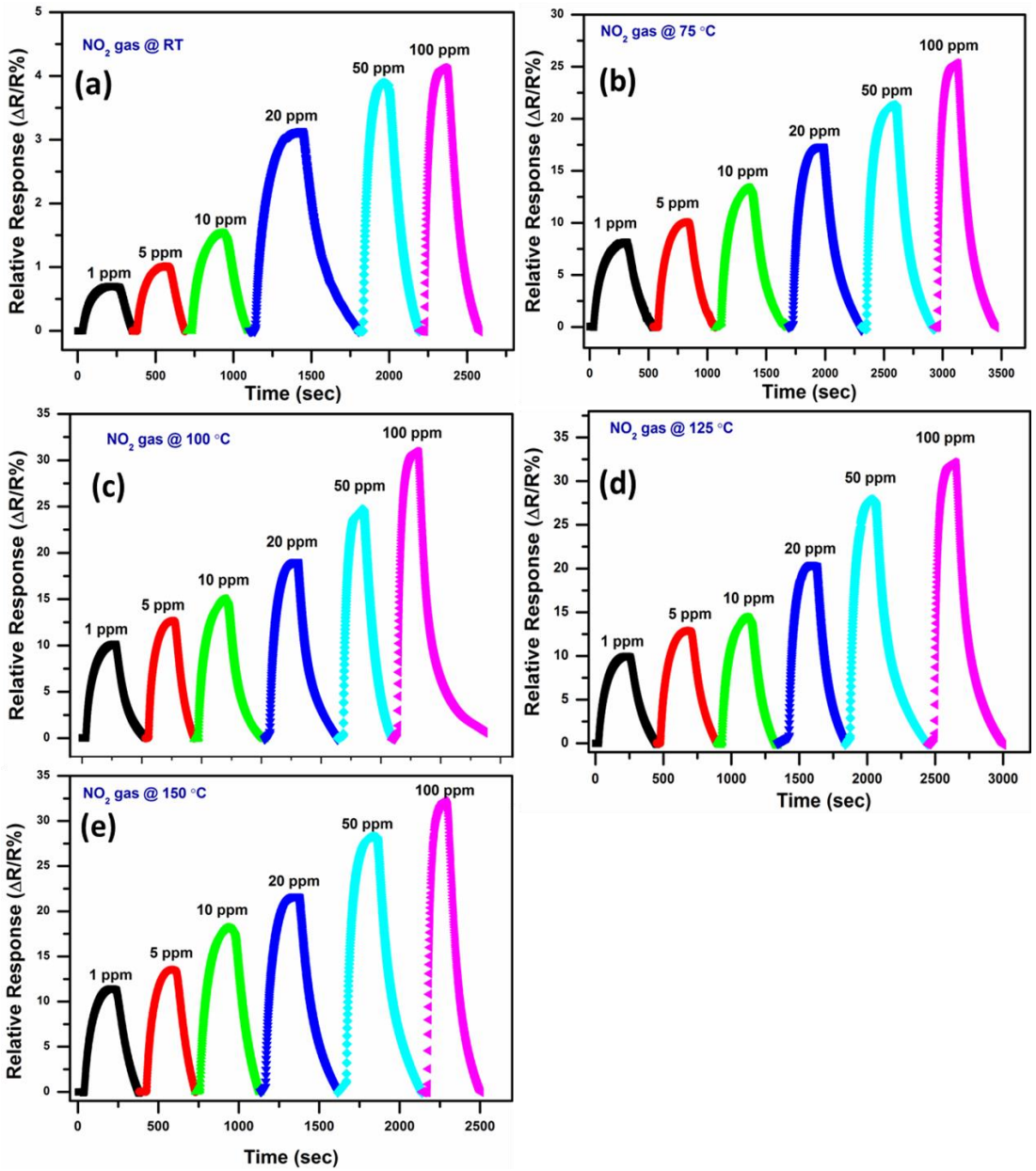

Figure 5.17: Relative response of V_2O_5 thin film towards NO_2 gas from 1 to 100 ppm at different temperatures (room temperature to 150 °C)

It is clearly seen that the response of NO_2 gas increases with higher concentration due to large surface reaction sites available for NO_2 gas at higher concentration. Relative response of V_2O_5

thin film has been observed ~ 32.5% for 100 ppm NO_2 at 150°C. Figure 5.18 shows the relative response of V_2O_5 thin film towards NO_2 gas, which increases up to 125°C, and then almost saturates at 150°C for 100 ppm.

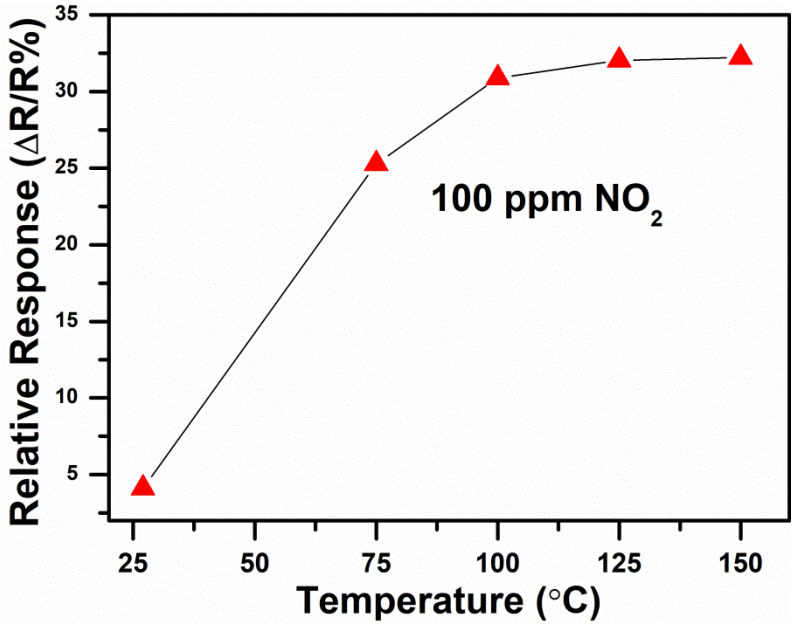

Figure 5.18: Comparison of relative response for V_2O_5 thin film towards 100 ppm of NO_2 gas at different temperatures

Thus, the saturated relative response is due to limited chemisorbed oxygen sites availability at 150°C working temperature. Furthermore, in order to investigate the effect of rGO on relative response, the rGO decorated on V_2O_5 thin film has been utilized for measuring the NO_2 gas from 1 to 100 ppm at 150°C, as shown in Figure 5.2.19 (a).

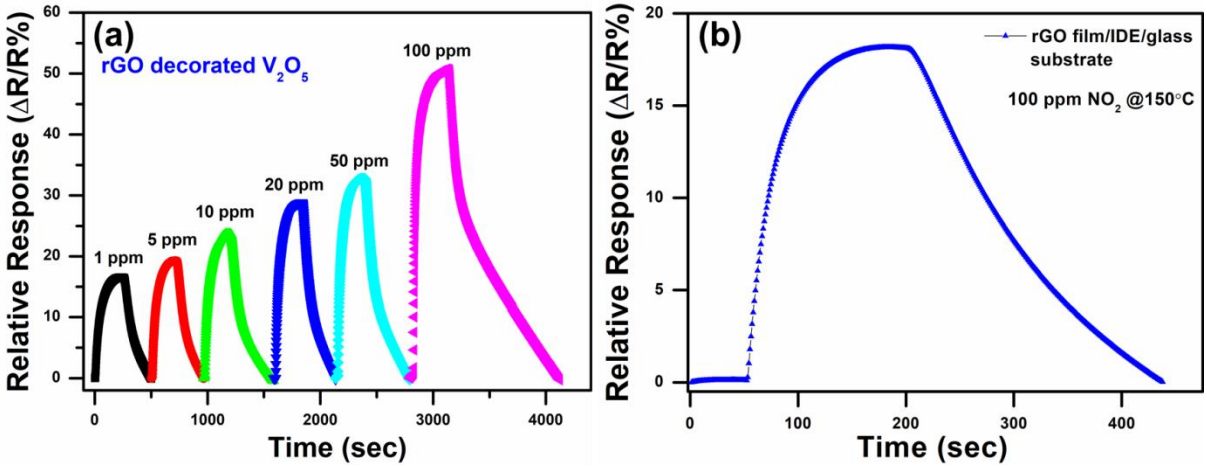

Figure 5.19: Relative response for NO_2 gas at 150 °C: (a) rGO-decorated V_2O_5 thin film and (b) rGO thin film/IDE/glass substrate

It is evident that the relative response increases to ~51% for 100 ppm at 150°C, while the relative response of rGO film decreases to 18.2% for 100 ppm at 150°C, as shown in Figure 5.19 (b). In order to examine the response and recovery kinetics of the sensor, we have calculated response time ~ 102.29 s and recovery time ~ 778.23 s for rGO decorated V_2O_5 thin film for 100 ppm NO_2 at 150°C, as shown in Figure 5.20.

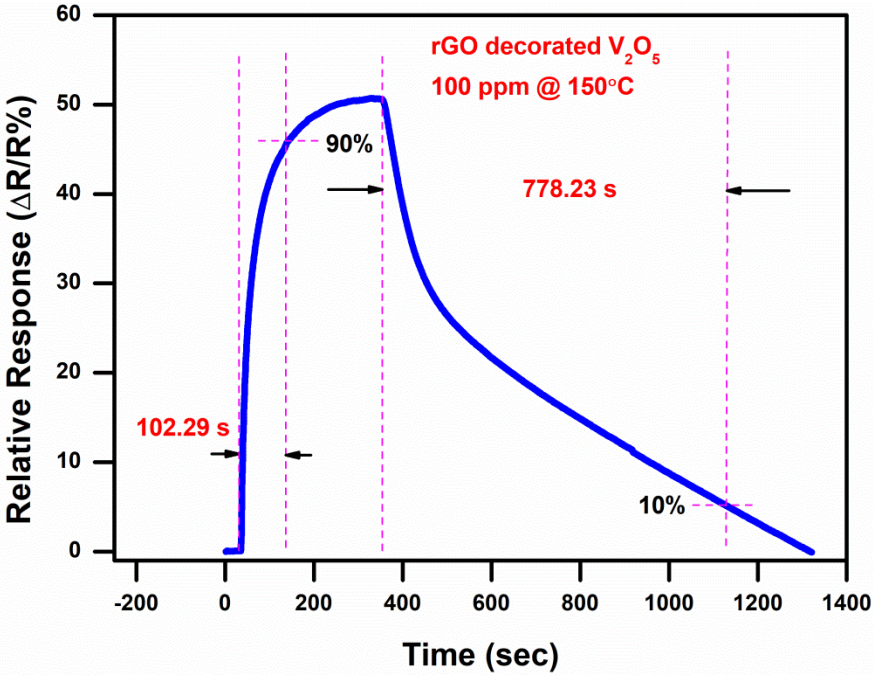

Figure 5.20: Response and recovery time calculation for rGO decorated V_2O_5 thin film for 100 ppm NO_2 gas at 150 °C

Basically, the response and recovery time are the key parameters for any sensor. The response time has been measured as the time required to obtain 90% of the saturation value during the loading of NO_2 gas into the sensor's chamber. Moreover, the recovery time has been calculated until the sensor's response is 10% of the saturation value during deloading of NO_2 gas. Sensor based on rGO decorated V_2O_5 thin films for NO_2 gas exhibits good sensor characteristics in terms of relative response, operating power, and working temperature. The sensor shows good relative response of 50.7% at mild temperature of 150°C. Apart from this, the sensor is operated at 32µW, which is the essential requirement of a gas sensor at low operating power. Figure 5.21 shows the comparison of all sensors in terms of their relative response towards 100 ppm NO_2 gas at 150°C.

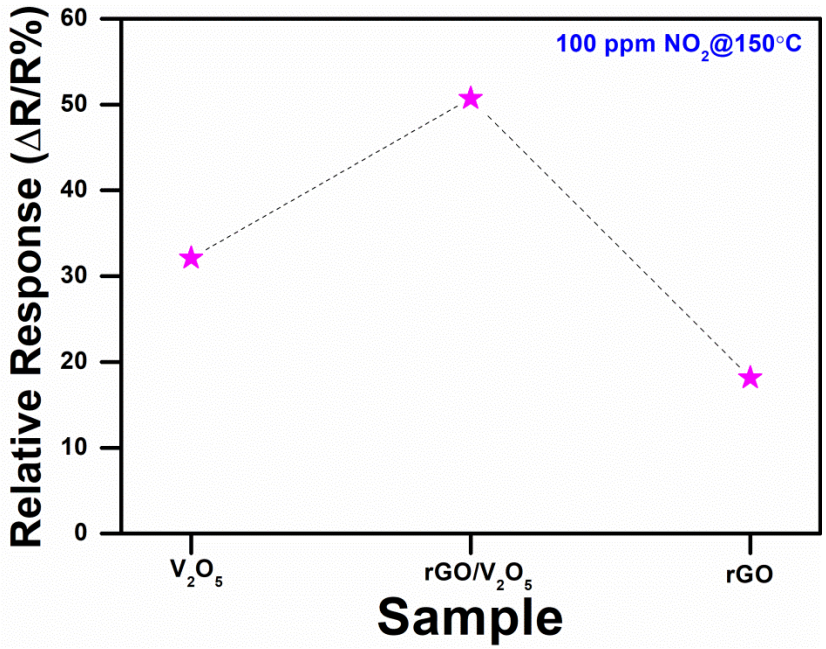

Figure 5.21: Comparison of relative response for V_2O_5 thin film, rGO film, and rGO-decorated V_2O_5 thin film for 100 ppm NO_2 gas at 150 °C

Hence, the relative response of rGO decorated V_2O_5 thin film is found to be more than other sensors at same operating conditions. Thus, rGO decorated V_2O_5 thin film based sensor for NO_2 gas exhibits 61% times improved relative response than V_2O_5 thin film. Sensing performance of different gas sensors for NO_2 gas is shown in Table 5.2, where comparison is shown with rGO decorated V_2O_5 thin film.

Table 5.2: Comparison of different NO_2 gas sensors with rGO decorated V_2O_5 thin film sensor

S.N	*Sensing material*	*Response*	*Conc. (ppm)*	*Temp. (°C)*	*Response time (s)*	*Recovery time (s)*	*References*
1.	n- type InP epitaxial layer	~0.08 ($\Delta R/R_o$)	0.1	100	180	-	Wierzbowska *et al.*, 2008
2.	Monolayer MoS_2	6.1% ($\Delta I/I$)%	1.2	RT	>1800	>1800	He *et al.*, 2012
3.	MoS_2	5.8 (R_a/R_g)	1	200	2460	2340	Donarelli *et al.*, 2015
4.	SnO_2/rGO	6.5 (R_g-R_a)/R_a	50	RT	190.2	223.8	Liu *et al.*, 2014
5.	WO_3 thin film	5 (R_a/R_g)	1	370	-	-	Stankova *et al.*, 2005
6.	SnO_2 NP-rGO (2D)	3.31 (R_a/R_g)	5	50	135	200	Zhang *et al.*, 2018
7.	Hierarchical SnO_2	~7 (R_g/R_a)	0.5	65	600	2760	Liu *et al.*, 2017
8.	rGO decorated V_2O_5 thin film	50.7% ($\Delta R/R$)%	100	150	102.29	778.23	This work

It can be observed that the sensing response of rGO decorated V_2O_5 (~16.52%) is higher at mild temperature even at 1 ppm NO_2 concentration. Generally, the MO_x based gas sensors are highly influenced by the water vapor. For this purpose, the relative humidity (RH) test on the rGO decorated V_2O_5 thin film has been performed. Figure 5.22 shows the variation of base line resistance with relative humidity from 10 to 50% RH at 150°C.

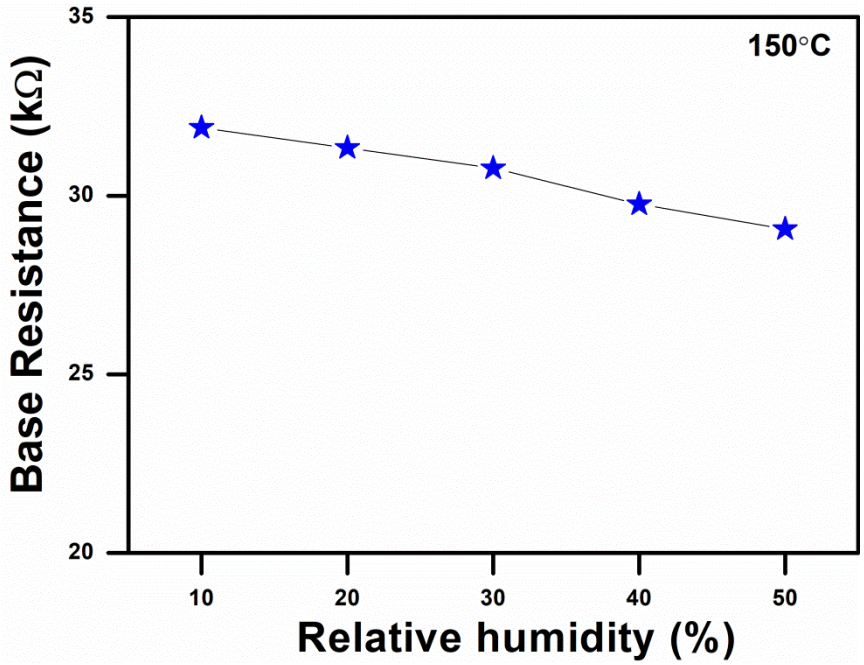

Figure 5.22: Variation of baseline resistance with relative humidity for rGO-decorated V_2O_5 thin film at 150 °C

These results indicate that the base resistance decreases very slightly with relative humidity at 150°C. The decrease in base line resistance with humidity is due to the adsorption of water vapor on the sensor's surface which reduces the number of electrons on the sensing layer. On the other hand, these adsorbed water vapors on sensor's surface result in less chemisorbed oxygen ions formation due to limited surface area. Consequently, the adsorption of NO_2 would also be slow due to formation of water vapor on sensor's surface which results in decrease in the relative response.

5.2.8 Gas Sensing Mechanism

The gas sensing mechanism of MO_x based gas sensor can be described by the surface adsorption and desorption of target gas molecules. It consequently changes the depletion layer, which in turn determines the relative response of gas sensor. When V_2O_5 thin films are exposed to atmospheric air, the chemisorbed oxygen ions (O_2^-, O^{2-}) are formed on the sensor's surface due to the removal of free electrons from the conduction band of V_2O_5 thin film (shown in Eqs. (5.2) and (5.3)).

$$O_{2(gas)} \rightarrow O_{2(ads\ on\ V2O5)} \tag{5.2}$$

$$O_{2(ads\ on\ V2O5} + e^- \rightarrow O_{2(V2O5)} \tag{5.3}$$

This increases the depletion layer of V_2O_5 thin film. However, the formation of chemisorbed oxygen ions on V_2O_5 thin film is strongly controlled by working temperature. When NO_2 gas is exposed on the sensor's surface, it reacts with chemisorbed oxygen ions, and takes more numbers of electrons from the conduction band of V_2O_5 thin film due to high electronegative nature of NO_2 gas (shown in Eq. (5.4)).

$$NO_{2(gas)} + O_2^- + 2e^- \rightarrow NO_2^- + 2O^- \tag{5.4}$$

This further increases the depletion layer on the sensor's surface. For the rGO decorated V_2O_5 thin film based sensors, which show enhanced relative response of NO_2 gas as compared to V_2O_5 thin film, an auxiliary mechanism for sensing enhancement should be highlighted. Moreover, rGO decorated V_2O_5 sensor also shows excellent relative response as compared to rGO film based sensor. Improvement in relative response can be understood by few extra mechanisms. Figure 5.23 (a-c) shows NO_2 sensing mechanism by using the idea of p-n

heterojunction with the band bending diagram. Firstly, V_2O_5 is a familiar n-type MO_x, and rGO shows p-type behavior. The work function of V_2O_5 and rGO is 3.61 and 4.90 eV, respectively. It is well known that the majority charge carriers in n-type V_2O_5 are electrons, and holes are majority charge carrier in p-type rGO. When both p-type rGO and n-type V_2O_5 combine with each other, the electrons will migrate from V_2O_5 to rGO, and holes will move towards V_2O_5 from rGO at the interface between p-type rGO, and n-type V_2O_5 until their Fermi levels attains an equilibrium condition. As a result, the movement of both charges in opposite direction cancels out each other at the interface, and forms a depletion layer between V_2O_5 and rGO. Therefore, the overall carrier concentration reduces, and resistance increases as depicted in *I-V* characteristics of rGO decorated V_2O_5 thin film in Figure 5.16 (a). Also, the band bending takes place due to creation of p-n heterojunction, as demonstrated in the band diagram of p-type rGO and n-type V_2O_5. When atmospheric air is exposed on rGO decorated V_2O_5 thin film based sensor, the electrons are extracted from the conduction band of V_2O_5 resulting in an increased width of the depletion layer at the p-n heterojunction, as shown in Figure 5.23 (b). Upon introduction of NO_2 gas molecules at the surface of rGO decorated V_2O_5 sensors, more numbers of electrons are ejected from the conduction band of V_2O_5 as well as oxygen ions by NO_2 gas. NO_2 gas is further converted into NO_2^- ions, resulting in increased width of p-n heterojunction that stimulates high relative response as compared to V_2O_5 thin film.

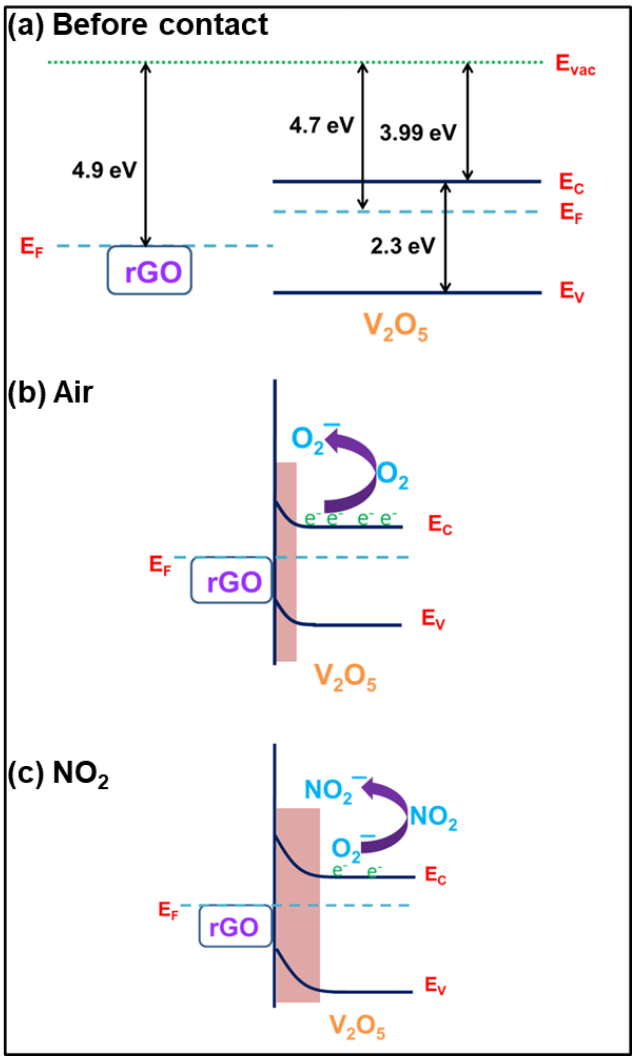

Figure 5.23: Schematic diagram of the sensing mechanism in the presence of air and NO_2 for rGO-decorated V_2O_5 thin film showing (a)–(c) band diagram illustrations of the p–n heterojunction before and after contact

Here, large number of heterojunctions are built up in rGO decorated V_2O_5 thin film, which correspondingly exhibit superior relative response towards NO_2 among all sensors. Secondly, the surface of rGO holds some defect sites, and functional groups which serve as active sites for

the incoming NO_2 gas molecules. Due to high electronegativity of NO_2 gas, it withdraws more number of electrons from oxygenous functional groups. This further increases the depletion layer of rGO decorated V_2O_5, leading to increased relative response of the sensor. The excellent relative response manifests that rGO decorated V_2O_5 thin film is a suitable candidate for NO_2 gas sensing applications.

5.3 CONCLUSION

The conclusion of the first part of this chapter describes about the highly sensitive hydrogen gas sensor based on rGO decorated onto Cr/Au IDE pattern over 4% Ni-doped ZnO nanostructures. Different concentration of rGO (0-1.5 wt%) on Ni-doped ZnO has been used to study the hydrogen sensing behaviour. Initially, resistance increases at low concentration of rGO (from 0 wt% to 0.75 wt%) decoration, and decreases when the concentration of rGO reaches (1.5 wt%) as observed by the *I-V* characteristics. Hydrogen gas sensors exhibit maximum relative response of ~63.8% for 100 ppm at 150°C with 0.75 wt% of rGO decorated on Ni doped ZnO nanostructures. The sensor exhibits excellent selectivity towards hydrogen gas in comparison with CH_4 and CO_2 gases even at lowest gas concentrations (1ppm to 100 ppm). The enhancement of relative response is mainly attributed to the existence of synergistic effect of maximum number of p-n heterojunction having large Schottky barrier height variations with more oxygen ions adsorption site availability on rGO for hydrogen gas. However, the decreased relative response with 1.5wt% decoration of rGO can be attributed to the formation of interconnected rGO between electrodes, reducing the total resistance and allowing the current flow directly through the interconnected rGO between electrodes. Thus, these p-n heterojunctions of 1.5 wt% rGO (p-type) with Ni doped ZnO (n- type) and other active site due to Ni dopant will no longer be effective for gas sensing response.

The second section of this chapter investigates the improved NO_2 gas sensing properties based on rGO decorated V_2O_5 thin film. DC sputtering system has been utilized to fabricate V_2O_5 thin film, and furthermore rGO is decorated by drop cast method. Initially, the current of rGO decorated V_2O_5 decreases more than V_2O_5 thin film, and later current is found to increase in the rGO film on glass substrate, which is also evident in the *I-V* characteristics. Moreover, a comparison has been made for the relative response of all sensors. Surprisingly, it is found that only rGO decorated V_2O_5 sensor marked highest NO_2 gas sensing response for 100 ppm at 150°C. Additionally, the above specified rGO decorated V_2O_5 sensor gives approximately 61% times more sensing response over the V_2O_5 thin film based sensor. The extremely high sensing response is due to the formation and modulation of p-n heterojunction at the interface of rGO and V_2O_5. Exceptionally, the presence of active sites like oxygenous functional groups on rGO surface also increases the sensing response.